Article

Discovery Medicine 2025; 37(201): 2388–2399
https://doi.org/10.24976/Discov.Med.202537201.202

STING/CXCL10 Axis Inhibits Macrophage M2 Polarization and BMCs Differentiation in Lung Cancer Cells

Haijian Liu[1], Danfei Zhou[1], Jiaojiao Ren[1], Jiangdong Li[1], Shanshan Hu[1], Jun Ying[1,*]

[1]Department of Respiratory and Critical Care Medicine, Ningbo No.2 Hospital, 315099 Ningbo, Zhejiang, China
*Correspondence: yingjun_yjun@163.com (Jun Ying)
Submitted: 4 July 2025 Revised: 10 September 2025 Accepted: 23 September 2025 Published: 20 October 2025

Objective: Macrophages and myeloid-derived suppressor cells (MDSCs) are key immune cells within the tumor microenvironment. Activation of the stimulator of interferon genes (STING) pathway and its downstream secretion of C-X-C motif chemokine ligand 10 (CXCL10) can suppress tumor development. This study investigated whether the STING–CXCL10 axis inhibits tumor progression by preventing macrophage M2 polarization and the differentiation of bone marrow cells (BMCs) into MDSCs.
Methods: Western blotting and quantitative reverse transcription-polymerase chain reaction (qRT-PCR) were used to assess the expression levels of STING and CXCL10. Lung cancer cell culture supernatants were collected and co-cultured with macrophages and bone marrow cells (BMCs). Flow cytometry was employed to evaluate macrophage polarization and the differentiation of MDSCs. Enzyme-linked immunosorbent assay (ELISA) was performed to measure CXCL10 levels in the lung cancer cell culture supernatant. To assess cell viability and invasion, BMCs or M0 macrophages were co-cultured with lung cancer cells, and the roles of STING and CXCL10 in these processes were analyzed.
Results: STING signal pathway is downregulated in lung cancer cell lines. Silencing of STING promotes macrophage M2 polarization and BMCs to MDSCs differentiation. In addition, knockdown of STING led to a downregulation of CXCL10 levels. Effects of STING overexpression were abolished by neutralizing antibody to CXCL10 (NAb-CXCL10). Co-culture of lung cancer cells with M0 macrophages or BMCs enhanced their viability and invasive capacity, whereas STING overexpression inhibited these effects by upregulating CXCL10.
Conclusions: This study suggests that the activation of the STING/CXCL10 axis inhibits macrophage M2 polarization and differentiation of BMCs to MDSCs. This study further suggests that the STING/CXCL10 axis is a potential target for lung cancer therapy.

Keywords: stimulator of interferon gene; C-X-C motif chemokine ligand 10; macrophage M2 polarization; myeloid-derived suppressor cells; lung cancer

Introduction

Lung cancer is a highly prevalent and deadly malignancy worldwide, and has become the second common cancer in the world, and the mortality rate is always high [1,2]. Lung cancer can metastasize throughout the body, with brain metastases being particularly common and associated with a poor prognosis. The tumor microenvironment (TME) plays a crucial role in the metastatic process of lung cancer [3]. Immune cells such as macrophages and myeloid-derived suppressor cells (MDSCs) are major components of the TME and can significantly promote the immune evasion of malignant tumor cells [4]. In the early stages of cancer, macrophages and bone marrow cells (BMCs) are recruited to form the tumor immune microenvironment around the tumor. In later stages, as cancer cell growth becomes uncontrolled, macrophages polarize from the anti-tumor M1 phenotype to the pro-tumor M2 phenotype, and BMCs differentiate into MDSCs, which not only contribute to tumor growth and progression but also significantly influence therapeutic efficacy and prognosis [5]. Therefore, targeting key components of the TME has emerged as a promising research direction for the treatment of lung cancer.

Activation of the stimulator of interferon gene (STING) signaling pathway facilitates the blockage of cancer metastasis. The anti-tumor properties of STING are attributed to its role in cancer-associated immune responses, remodeling of the TME, and the eventual elimination of tumor cells [6,7]. STING agonists are primarily used in tumor immunotherapy, where activation of STING in tumor cells promotes interferon (IFN) production and initiates T cell responses [8]. In BRCA1-deficient breast cancer cells, poly (ADP-ribose) polymerase (PARP) inhibitors stimulate the release of double-stranded DNA (dsDNA) fragments, which are detected by STING sensors within tumor

Copyright: © 2025 The Author(s). Published by Discovery Medicine. This is an open access article under the CC BY 4.0 license.
Note: *Discovery Medicine* stays neutral with regard to jurisdictional claims in published maps and institutional affiliations.

cells, leading to increased type I interferons (IFN-I) production and activation of $CD8^+$ T cell-mediated anti-tumor responses [9]. In contrast, the catalytic degradation of cytoplasmic DNA can suppress STING-dependent immune activation in cancer cells [10]. Therefore, STING-mediated immune activation within the TME remains a promising area of investigation.

STING was found to inhibit small cell lung cancer progression by stimulating IFN-gamma-inducible protein 10 (CXCL10), which recruits immune T cells [11]. CXCL10 is a ligand for C-X-C motif chemokine receptor 3 (CXCR3) and exerts its biological effects through the binding of both. In lung cancer, the upregulation of CXCL10 by high mobility group protein A2 (HMGA2) recruits $CD8^+$ T cells and thus exerts anti-tumor effects [12]. In addition, CXCL10 has been shown to act as a ligand for CXCR3 and correlate with the infiltrative capacity of tumor-infiltrating lymphocytes [13]. In lung cancer, Jie *et al.* [14] found that CXCL10 enhanced the killing effect of $CD8^+$ T cells. In the TME, the programmed cell death protein 1 (PD1)/programmed cell death-ligand 1 (PD-L1) axis attenuated the killing effect of $CD8^+$ T cells by inhibiting their cytokine production and cell migration [15]. This indicates that the mechanism by which CXCL10 restores the killing effect of $CD8^+$ T cells on tumor cells is also a topic of further investigation.

This study aims to explore the immunoregulatory mechanism of the STING–CXCL10 axis within the tumor microenvironment, with a particular focus on its synergistic effects on macrophage polarization and the differentiation of MDSCs. Previous research has shown that STING activation can enhance anti-tumor immunity through the induction of CXCL10. However, whether this pathway simultaneously reshapes the tumor immune microenvironment by inhibiting M2-type macrophage polarization and the differentiation of bone marrow cells into MDSCs remains unclear. This study will systematically investigate the key role of STING–CXCL10 signaling in regulating immune cell fate, with the goal of providing a new molecular basis for developing lung cancer treatment strategies targeting the STING pathway.

Materials and Methods

Animal Ethics

Thirteen male C57BL/6J mice (6–8 weeks old, 20–25 g) were obtained from Hangzhou Medical College (Zhejiang, China) and housed under controlled conditions (20–26 °C, 40–70% humidity) with free access to food and water on a 12-hour light/dark cycle. All animal procedures were conducted in accordance with the guidelines of the China Council on Animal Care and Use and were approved by the Ethics Committee of Zhejiang Baiyue Biotech Co., Ltd. for Experimental Animals Welfare (NO. ZJBYLA-IACUC-20230622).

Cell Culture

All mouse lung cancer cell lines—D122 (CVCL_0242, Cellosaurus, Lausanne, Switzerland), BC215 (CVCL_Y281, Cellosaurus, Lausanne, Switzerland), and A9 (CVCL_S007, Cellosaurus, Lausanne, Switzerland)—as well as the mouse lung epithelial cell line MLE-12 (AW-CM0081, Anweisci, Shanghai, China), were cultured in Dulbecco's Modified Eagle Medium/Nutrient Mixture F-12 (DMEM/F12) 50/50 medium (10-092-CV, Corning, NY, USA), supplemented with 10% fetal bovine serum (FBS; 35-081-CV, Corning Incorporated, Corning, NY, USA), 2 mM L-glutamine (99-595-CM, Corning Incorporated, Corning, NY, USA), 100 IU/mL penicillin (61-238-RM, Corning Incorporated, Corning, NY, USA), and 100 µg/mL streptomycin (HY-B1906, MCE, NJ, USA), and maintained until reaching 100% confluency. Mouse RAW 264.7 cells (AW-CM0088, Anweisci, Shanghai, China) were cultured in RPMI-1640 medium (11875093, Thermo Fisher, Waltham, MA, USA) supplemented with 10% FBS, 0.05 mM β-mercaptoethanol (31350010, Thermo Fisher, Waltham, MA, USA), 1% penicillin/streptomycin (P/S), and 4.5 g/L dextrose. RAW 264.7 cells were then stimulated with 20–100 ng/mL phorbol 12-myristate 13-acetate (PMA; HY-18739, MCE, NJ, USA) overnight to induce differentiation into non-committed M0 macrophages [16]. MLE-12 and RAW 264.7 cells were short tandem repeat (STR) verified by the supplier, and all cell lines tested negative for mycoplasma contamination. Mycoplasma testing confirmed negative results for all cell lines: D122, BC215, and A9. D122 and BC215 cells exhibited epithelium-like adhesion growth, while A9 cells displayed fibroblast-like morphology. All cell lines were in good condition with no contamination detected.

Primary bone marrow cells (BMCs) were isolated from the femurs of mice. Animals were sacrificed by intraperitoneal injection of 2% pentobarbital sodium (100 mg/kg). The bilateral femurs were then aseptically excised, with attached muscles and connective tissues removed, and both ends of the femurs cut off. Bone marrow was flushed into cold phosphate-buffered saline (PBS) (10010023, Thermo Fisher, Waltham, MA, USA) supplemented with 2% heat-inactivated FBS using a syringe. The cells were repeatedly flushed up and down 4–6 times to dissociate them. Cell clumps and debris were removed by passing the suspension through a 70 µm filter. The resulting cell suspension was then treated with three volumes of 0.8% NH4Cl and incubated on ice for 10 minutes to lyse red blood cells. The cells were centrifuged at low temperatures for 5 min and resuspended with cold PBS+2% inactivated FBS [17]. All cells tested negative for mycoplasma. The identity of primary BMCs was confirmed based on their characteristic morphology observed under a microscope and the analysis of cell-specific surface markers by flow cytometry.

Table 1. The primer sequences of related genes.

Gene	Forward primer (5′-3′)	Reverse primer (5′-3′)
STING (mouse)	GCCAGCCTGATGATCCTTTG	GGCCAAACATCCAACTGAGG
GAPDH (mouse)	AGTGTTTCCTCGTCCCGTAG	CATTCTCGGCCTTGACTGTG

STING, stimulator of interferon genes; *GAPDH*, glyceraldehyde-3-phosphate dehydrogenase.

Table 2. Antibodies used in this study.

Name	Catalog	Molecular weight	Dilution	Manufacturer
CXCL10	ab271208	10 kDa	1/1000	abcam, UK
p-STING	PA5-105674	40 kDa	1/1000	Invitrogen, USA
STING	ab189430	42 kDa	1/1000	abcam, UK
GAPDH	ab8245	37 kDa	1/1000	abcam, UK
Goat anti mouse	ab205719	—	1/2000	abcam, UK
Goat anti rabbit	31460	—	1/5000	Thermo Fisher, USA

CXCL10, IFN-gamma-inducible protein 10; STING, stimulator of interferon gene; p-STING, phospho-STING; GAPDH, glyceraldehyde-3-phosphate dehydrogenase.

Transfection

Cells were seeded in 24-well culture plates at a density of 1.0×10^5 cells per well and incubated for 24 h. The transfection mixture consisted of 1.2 µL FuGENE® 6 transfection reagent (F6-1000, Neobioscience, San Diego, CA, USA), 18.8 µL OPTI-MEM medium (31985088, Thermo Fisher, Waltham, MA, USA), and either STING overexpression plasmid (Yunzhou Biosciences Co., Ltd., Guangzhou, China), negative control (NC), short hairpin STING (shSTING: 5′-AGAGGTCACCGCTCCAAATAT-3′) (Yunzhou Biosciences Co., Ltd., Guangzhou, China), or short hairpin RNA negative control (shNC: 5′-CAACAAGATGAAGAGCACCAA-3′). This mixture was immediately added to the cells for transient transfection. The coding sequence (CDS) region of STING is provided in the **supplementary materials**. Following transfection, cells were incubated for an additional 48 h at 37 °C in a humidified atmosphere containing 95% air and 5% CO_2 before analysis of transfection efficiency.

Quantitative Reverse Transcription-Polymerase Chain Reaction (qRT-PCR) Analysis

The total RNA was extracted using TRIzol Reagent (A33251, Thermo Fisher, Waltham, MA, USA). RNA quality was tested using NanoDrop One (840-317400, Thermo Fisher, Waltham, MA, USA). The cDNA was obtained by cDNA synthesis kit (6210A, Takara, Kusatsu, Shiga, Japan). TB Green® Fast qPCR Mix (RR430S, Takara, Kusatsu, Shiga, Japan) was added into cDNA for qRT-PCR. The results were analyzed using qRT-PCR instrument (V514732, Thermo Fisher, Waltham, MA, USA). The relative mRNA expression levels were calculated using the $2^{-\Delta\Delta CT}$ method [18] and normalized to an internal reference (glyceraldehyde-3-phosphate dehydrogenase (*GAPDH*)). All primer sequences are summarized in Table 1.

Western Blotting

Proteins were isolated from cells using a commercial kit (BB-31013, Bestbio, Shanghai, China). Protein concentration was determined with a Bicinchoninic Acid (BCA) Protein Assay Kit (P0012, Beyotime, Shanghai, China). For subsequent analysis, 30 µg of protein was loaded per sample. Proteins were separated by sodium dodecyl sulfate–polyacrylamide gel electrophoresis (SDS-PAGE) (P0690, Beyotime, Shanghai, China) and transferred onto polyvinylidene fluoride (PVDF) membranes (FFP24, Beyotime, Shanghai, China). Membranes were blocked with 5% bovine serum albumin (BSA) (ST025, Beyotime, Shanghai, China). After washing, membranes were incubated overnight at 4 °C with primary antibodies. GAPDH served as the endogenous loading control. Membranes were then incubated with appropriate horseradish peroxidase (HRP)-conjugated secondary antibodies for 1 h. Protein bands were visualized using enhanced chemiluminescence (ECL) reagent (P0018AS, Beyotime, Shanghai, China) and imaged with the BeyoImage™600 Chemiluminescent Imaging System (EI600, Beyotime, Shanghai, China). All antibodies used are listed in Table 2. Band intensities were quantified using ImageJ software and normalized to GAPDH. Data are presented as fold change relative to the control group.

Co-Culture of A9/D122 Cells Supernatant With RAW 264.7 Cells or BMCs

The experiments were divided into the following groups: M0, M0+A9, M0+A9+NC, M0+A9+STING, M0+A9+shNC, M0+A9+shSTING, and M0+A9+STING with neutralizing antibody to CXCL10 (NAb-CXCL10). RAW 264.7 cells in the M0 group were induced into M0 macrophages as described above. In the M0+A9 group, A9 culture supernatant was co-cultured with M0 macrophages in 6-well plates at a total volume of 2

mL per well for 72 hours [16]. For the M0+A9+NC, M0+A9+STING, M0+A9+shNC, M0+A9+shSTING, and M0+A9+STING+NAb-CXCL10 groups, A9 cells were transfected with the respective plasmids and cultured for 48 hours. The resulting culture supernatants were then collected and co-cultured with M0 macrophages in 6-well plates (2 mL per well) for 72 hours. In the M0+A9+STING+NAb-CXCL10 group, the neutralizing antibody to CXCL10 (NAb-CXCL10; 0.1 mg, BE0440, Bioxcell, Lebanon, NH, USA) was additionally added [19].

The experiments were divided into the following groups: BMC, BMC+D122, BMC+D122+NC, BMC+D122+STING, BMC+D122+shNC, BMC+D122+shSTING, and BMC+D122+STING+NAb-CXCL10. In the BMC group, bone marrow cells (BMCs) were cultured under normal conditions. For the BMC+D122 group, D122 cells were cultured for 48 hours, and the culture supernatant was collected. Then, 2 mL of this supernatant was added to BMCs in 6-well plates, and co-cultured for 72 hours. In the BMC+D122+NC, BMC+D122+STING, BMC+D122+shNC, BMC+D122+shSTING, and BMC+D122+STING+NAb-CXCL10 groups, D122 cells were transfected with the respective plasmids and cultured for 48 hours. The culture supernatant was collected and added to BMCs in 6-well plates (2 mL per well) for co-culture over 72 hours. In the BMC+D122+STING+NAb-CXCL10 group, neutralizing antibody to CXCL10 (NAb-CXCL10; 0.1 mg) was additionally added. After co-culture, macrophages and BMCs were collected for flow cytometry analysis.

Flow Cytometry

After macrophages were co-cultured with culture supernatant for 72 h, co-cultured macrophages were then stained with CD206 Alexa Flour 488 (C068C2, BioLwgend, San Diego, CA, USA) and CD163 Pecy7 (S15049F, BioLwgend, San Diego, CA, USA). After staining, cells were washed twice with PBS. Flow cytometry data were acquired using a BD LSRII cytometer (644788, BD, USA), and analysis was performed with FlowJo X software (version 10.8.1; BD Life Sciences, Ashland, OR, USA). MDSCs were identified using the markers Ly6C Alexa Fluor 488 (HK1.4, BioLegend, USA) and purified Ly6G (S19018G, BioLegend, San Diego, CA, USA); all other procedures remained consistent. For experiments involving a neutralizing antibody, the antibody was purified from the culture supernatant and conjugated to R-phycoerythrin (R-PE). After removing free R-PE, flow cytometry detection was performed.

Enzyme-Linked Immunosorbent Assay (ELISA)

An ELISA kit (ab260067, abcam, Cambridge, UK) specific for the detection of mouse CXCL10 was used. Supernatants were collected and experiments were performed according to the manufacturer's instructions. Finally, the absorbance of the samples was read at 450 nm using a microplate reader (1681135, Bio-Rad Laboratories, Shanghai, China).

Co-Culture of A9/D122 Cells With RAW 264.7 Cells or BMCs

As the subsequent experiments need to detect the vitality and invasion of cancer cells, co-culture was performed using Transwell chambers (FTW001, Beyotime, Shanghai, China). A9 cells were divided into the following groups: A9, M0+A9, M0+A9+NC, M0+A9+STING, and M0+A9+STING+NAb-CXCL10. In the A9 group, A9 cells were cultured under normal conditions. In the M0+A9, M0+A9+NC, M0+A9+STING, and M0+A9+STING+NAb-CXCL10 groups, M0 macrophages were placed in the upper chamber, and A9 cells transfected with the corresponding plasmids were placed in the lower chamber, with no direct cell contact between the two. In the M0+A9 group, the lower chamber contained untreated A9 cells, while the M0+A9+STING+NAb-CXCL10 group added 0.1 mg NAb-CXCL10 to the lower chamber.

D122 cells were divided into the following groups: D122, BMC+D122, BMC+D122+NC, BMC+D122+STING, and BMC+D122+STING+NAb-CXCL10. In the D122 group, D122 cells were cultured under normal conditions. For the BMC+D122, BMC+D122+NC, BMC+D122+STING, and BMC+D122+STING+NAb-CXCL10 groups, BMCs were seeded in the upper Transwell chamber, while D122 cells transfected with the respective plasmids were seeded in the lower chamber. In the BMC+D122 group, untreated D122 cells were placed in the lower chamber. In the BMC+D122+STING+NAb-CXCL10 group, 0.1 mg of neutralizing antibody to CXCL10 (NAb-CXCL10) was added to the lower chamber. All Transwell co-cultures were incubated for 1.5 days.

Cell Counting Kit-8 (CCK-8) Analysis

Following the manufacturer's instructions, A9 or D122 cells (3000 cells/well) were seeded into 96-well plates (FCP962, Beyotime, Shanghai, China). Cell viability was assessed using the CCK-8 (C0038, Beyotime, Shanghai, China). After adding 10 µL of CCK-8 reagent, the cells were incubated for 2 hours, and then the absorbance at 450 nm was measured using a microplate reader (Bio-Rad, Hercules, CA, USA).

Transwell Investigation

The upper chamber of the Transwell insert was coated with a uniformly diluted Matrigel (C0372, Beyotime, Shanghai, China) and allowed to solidify for 30 minutes. A total of 200 µL of A9 or D122 cell suspension (1×10^5 cells/mL) was added to the upper chamber, while 600 µL of culture medium containing 20% FBS was added to the

lower chamber. The chambers were incubated at 37 °C with 5% CO_2 for 24 hours. After incubation, the Transwell insert was removed, and cells and Matrigel remaining in the upper chamber were gently wiped away. The insert was then fixed with methanol (C06901102, Nanjing Reagent, Nanjing, China) for 30 minutes, followed by staining with 0.1% crystal violet (C0121, Beyotime, Shanghai, China) for another 30 minutes. Invaded cells were counted under a Olympus CKX53 microscope at 200× magnification (Olympus, Center Valley, PA, USA). The number of invaded cells was determined by counting three random fields per well and normalized to the control group (untreated cells, set as 100%).

Statistical Analysis

The one-way ANOVA was used for comparison among multiple groups, and Tukey's method was used for post hoc tests. Data were described by mean ± standard deviation, which was calculated by GraphPad 8.0 (Graphpad Software Inc., San Diego, CA, USA). And differences were considered statistically significant at $p < 0.05$.

Results

STING Is Downregulated in Lung Cancer Cell Lines

Mouse lung cancer cell lines D122, BC215, and A9 were selected to assess STING expression. The results showed that *STING* mRNA levels were significantly downregulated in these lung cancer cell lines compared to mouse lung epithelial cells (MLE-12) (Fig. 1A, $p < 0.001$). Subsequently, expression levels of STING pathway-related proteins were analyzed by western blotting. While total STING protein expression remained unchanged, the ratio of phosphorylated STING to total STING (p-STING/STING) was significantly lower in lung cancer cell lines than in MLE-12 cells (Fig. 1B, $p < 0.001$). A9 cells were then transfected with either STING-silencing or STING-overexpression plasmids, resulting in successful downregulation and upregulation of STING expression, respectively (Fig. 1C, $p < 0.001$). These findings indicate that the activity of the STING signaling pathway is reduced in lung cancer cells, suggesting a potential role for STING in regulating tumor progression.

Silencing of STING Promotes Macrophage M2 Polarization and Downregulates CXCL10

To investigate the effect of STING downregulation on macrophages in the lung TME, A9 cell culture supernatants were collected and co-cultured with RAW 264.7 M0 macrophages. Flow cytometry analysis revealed that co-culture with lung cancer cells promoted macrophage M2 polarization. Knockdown of STING further enhanced M2 polarization, whereas STING overexpression significantly reduced it (Fig. 1D, $p < 0.001$). To explore the role of the regulatory factor CXCL10, ELISA was used to measure CXCL10 levels in A9 culture supernatants. STING overexpression upregulated CXCL10, while silencing STING downregulated it (Fig. 1E, $p < 0.05$). Next, CXCL10 expression during macrophage polarization was assessed. Upon co-culture with A9 cells, CXCL10 was upregulated in macrophages with STING overexpression, whereas STING knockdown resulted in CXCL10 downregulation (Fig. 1F, $p < 0.05$). These findings suggest that silencing STING reduces CXCL10 secretion and promotes macrophage M2 polarization, thereby contributing to the immunosuppressive tumor microenvironment.

Silencing of STING Promotes BMCs to MDSCs Differentiation and Downregulates CXCL10

Continuing to investigate the effects of STING downregulation on MDSCs in the lung TME, D122 cell culture supernatants were collected and co-cultured with BMCs. Consistent with previous findings, STING knockdown and overexpression plasmids were transfected into D122 cells (Fig. 2A, $p < 0.001$). The identity of the primary BMCs was confirmed by their characteristic morphology and analysis of cell-specific surface markers via flow cytometry (Fig. 2B,C). Primary mouse bone marrow cells form a heterogeneous population, primarily composed of adherent fibroblast-like stromal cells, round hematopoietic stem cells, and lymphoblast-like lymphocytes (Fig. 2B). Flow cytometry analysis revealed that neutrophils constitute the largest proportion in primary mouse bone marrow cells, followed by B cells, myeloid progenitor cells, and hematopoietic stem cells. This cellular composition aligns with the typical features of normal mouse bone marrow, demonstrating successful isolation of primary cells with expected biological activity (Fig. 2C). Flow cytometry results demonstrated that co-culture promoted BMC differentiation toward MDSCs, and knockdown of STING similarly enhanced this differentiation, whereas STING overexpression inhibited BMC differentiation into MDSCs (Fig. 2D, $p < 0.001$). ELISA detection of CXCL10 levels in D122 culture supernatant showed that STING overexpression upregulated CXCL10, while STING knockdown downregulated it (Fig. 2E, $p < 0.01$). Furthermore, CXCL10 expression in BMCs was increased by STING overexpression and decreased by STING knockdown (Fig. 2F, $p < 0.05$). These results suggest that co-culture and STING silencing promote BMC differentiation into MDSCs, whereas STING overexpression, via upregulation of CXCL10, inhibits this process.

STING Overexpression Suppresses Tumor Progression via CXCL10-Mediated Pathways

To investigate the effect of the cytokine CXCL10 on macrophage polarization and BMC differentiation toward MDSCs, we added a neutralizing antibody against CXCL10 (NAb-CXCL10) to a co-culture system involving STING-overexpressing cancer cells. Flow cytometry

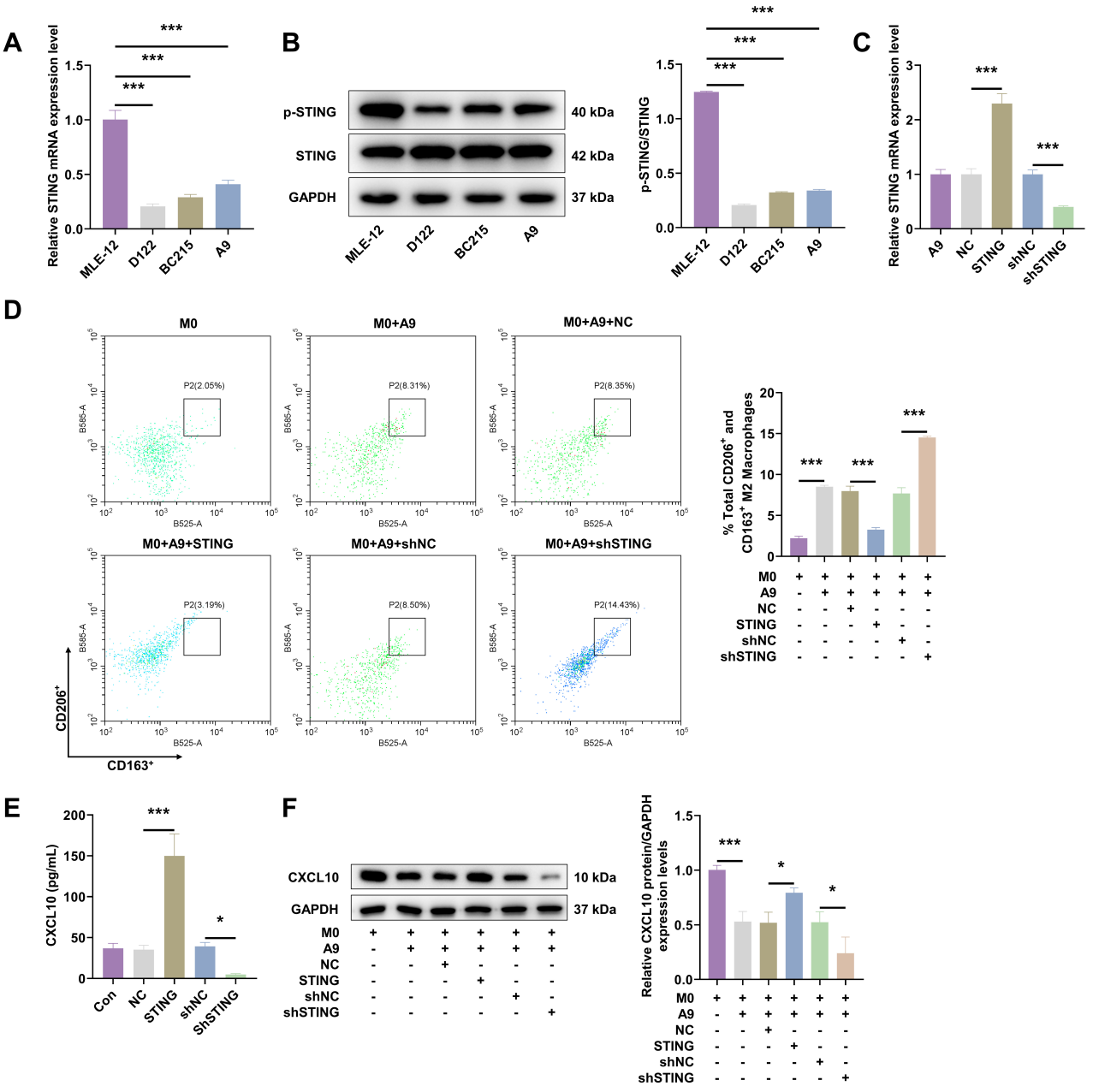

Fig. 1. STING is lowly expressed in lung cancer and silencing of STING promotes macrophage M2 polarization and downregulates CXCL10. (A) Expression of *STING* in various lung cancer cell lines (D122, BC215, A9) was detected by qRT-PCR. (B) Expression of STING protein in various lung cancer cell lines (D122, BC215, A9) was detected by WB. (C) The expression of *STING* in A9 cells was detected by qRT-PCR. (D–F) M0 macrophages were co-cultured with A9 lung cancer cell culture supernatants. (D) Detection of M2 macrophage polarization was assessed by flow cytometry. (E) CXCL10 levels in the A9 culture supernatant were measured by ELISA. (F) CXCL10 protein expression in macrophages was detected by WB. STING, stimulator of interferon gene; CXCL10, IFN-gamma-inducible protein 10; qRT-PCR, quantitative reverse transcription-polymerase chain reaction; WB, western blotting; ELISA, enzyme-linked immunosorbent assay; NC, negative control. GAPDH (glyceraldehyde-3-phosphate dehydrogenase) was used as an endogenous control in qRT-PCR and WB. Data are presented as mean ± SD (n = 3). *$p < 0.05$, ***$p < 0.001$.

results showed that NAb-CXCL10 reversed the inhibitory effect of STING overexpression on M2 macrophage polarization (Fig. 3A, $p < 0.001$). Co-culture with M0 macrophages promoted A9 cell viability and invasion (Fig. 3B,C, $p < 0.01$). STING overexpression suppressed these effects, while NAb-CXCL10 reversed the suppression (Fig. 3B,C, $p < 0.01$). Similarly, STING overexpression inhibited MDSC differentiation, and this effect

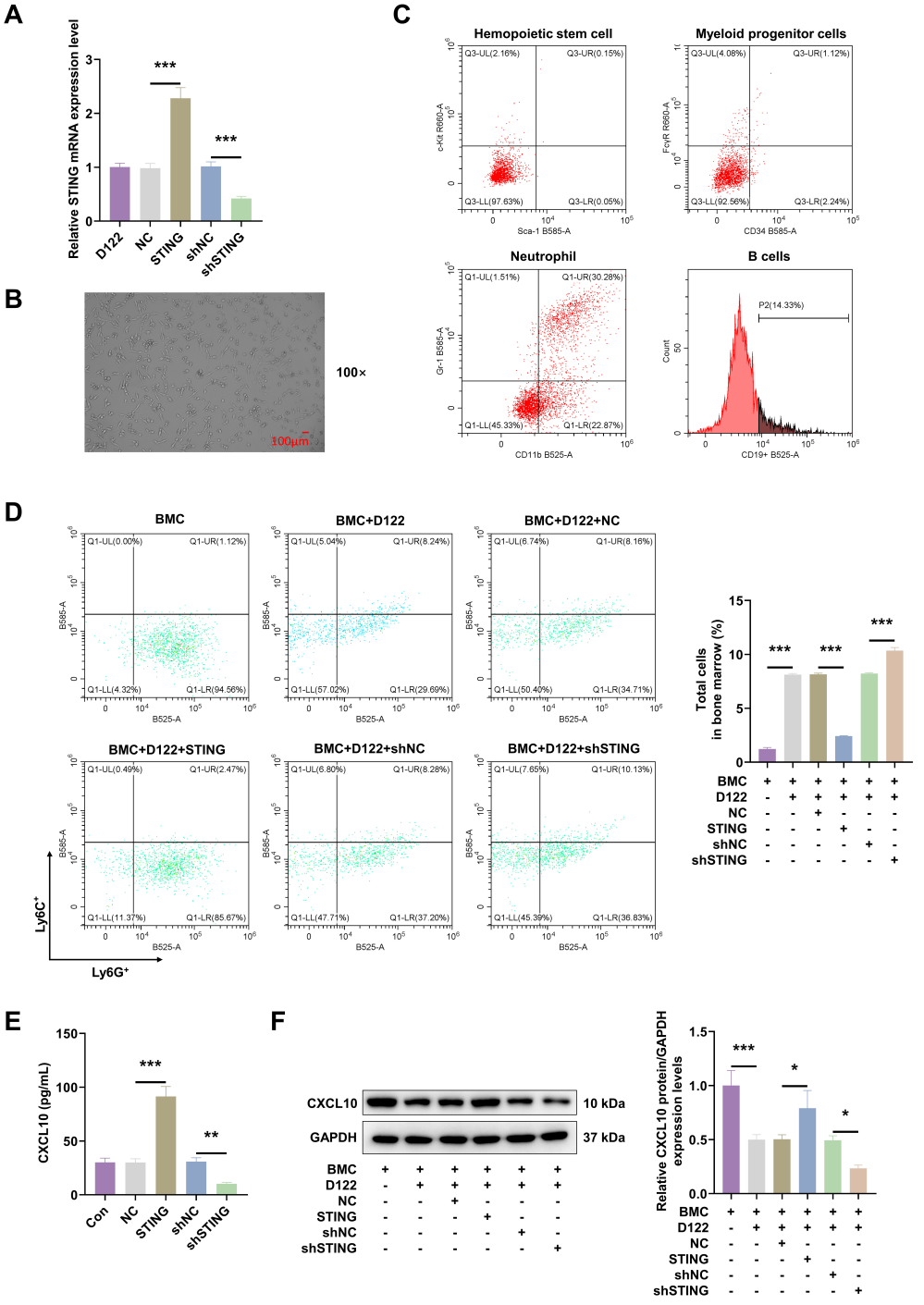

Fig. 2. Silencing of STING promotes BMCs to MDSCs differentiation and downregulates CXCL10. (A) *STING* expression in D122 cells was detected by qRT-PCR. (B) Morphology of BMCs was observed under an inverted microscope at 100× magnification (scale bar: 100 μm). (C) Surface markers of BMCs were identified by flow cytometry. (D–F) BMCs were co-cultured with D122 lung cancer cell culture supernatants. (D) Differentiation of BMCs into MDSCs was assessed by flow cytometry. (E) CXCL10 levels in the D122 culture supernatant were measured by ELISA. (F) CXCL10 protein expression in BMCs was detected by WB. STING, stimulator of interferon gene; CXCL10, IFN-gamma-inducible protein 10; BMC, bone marrow cell; MDSC, myeloid-derived suppressor cell; ELISA, enzyme-linked immunosorbent assay; WB, western blotting; NC, negative control. GAPDH was used as an endogenous control in WB. Data are presented as mean ± SD (n = 3). *$p < 0.05$, **$p < 0.01$, ***$p < 0.001$.

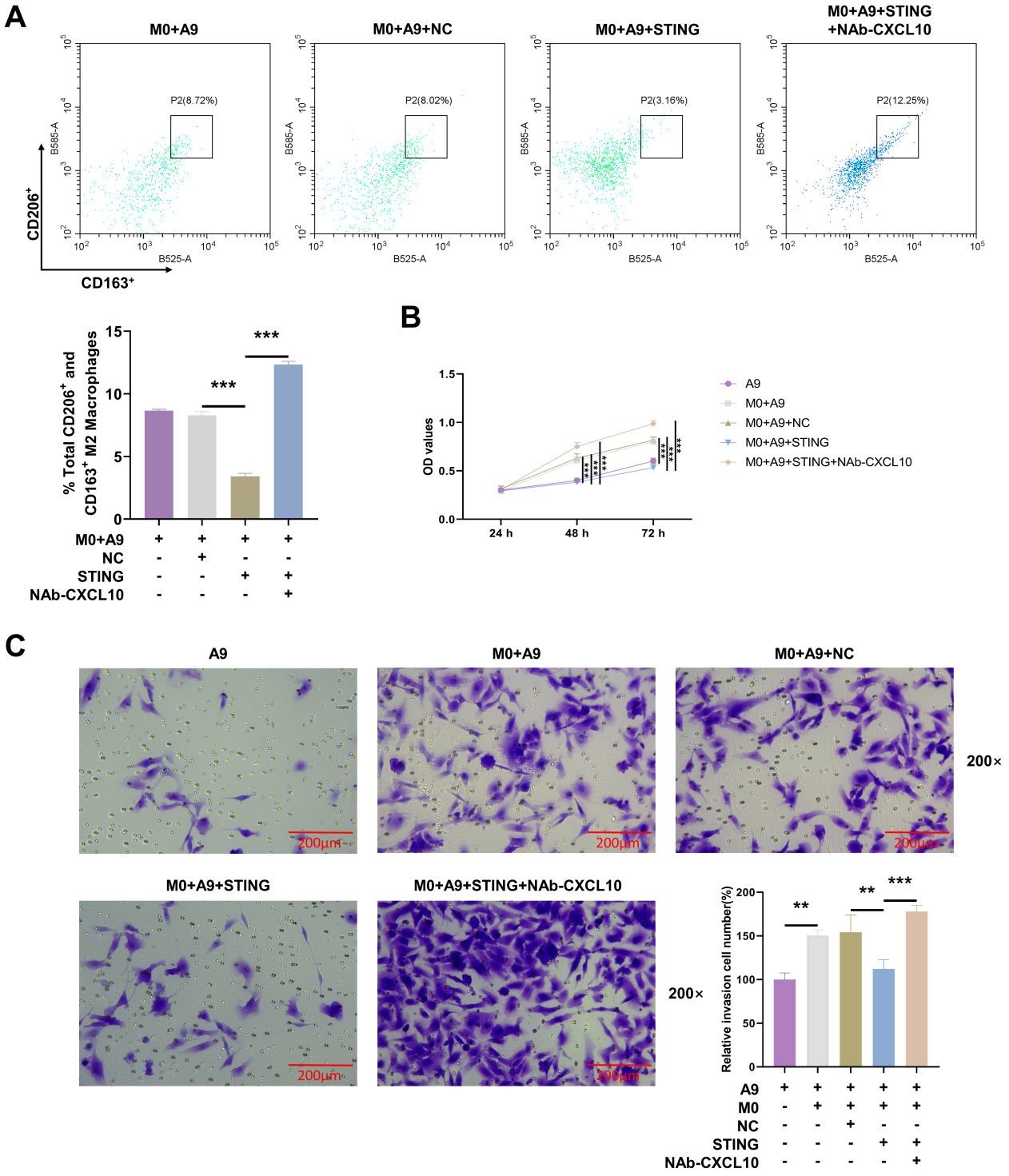

Fig. 3. Regulation of M2 macrophage and lung cancer progression by CXCL10 blockade and STING overexpression. (A) M0 macrophages and A9 lung cancer cell culture supernatants were co-cultured with CXCL10 neutralizing antibody, and M2 macrophage polarization levels were assessed by flow cytometry. (B) The viability of A9 cells co-cultured with M0 macrophages and CXCL10 neutralizing antibody was measured using the CCK-8 assay. (C) A9 cell invasion was evaluated by Transwell assay under the same co-culture conditions with CXCL10 neutralizing antibody, and the invasion rate was quantitatively analyzed. Representative images were captured at 200× magnification with a scale bar of 200 μm. STING, stimulator of interferon gene; CXCL10, IFN-gamma-inducible protein 10; CCK-8, cell counting kit-8. Data are presented as mean ± SD (n = 3). $^{**}p < 0.01$, $^{***}p < 0.001$.

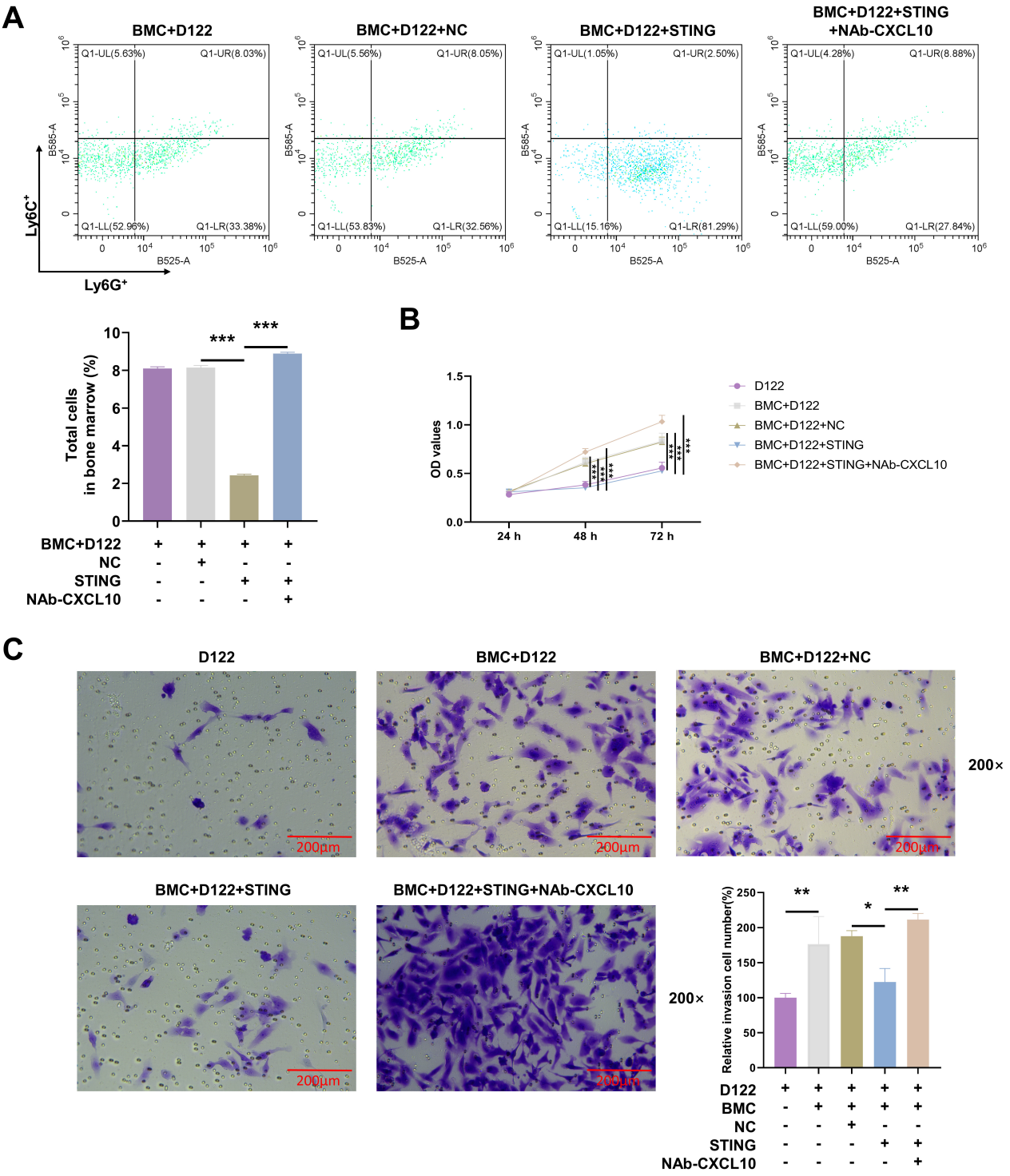

Fig. 4. Regulation of MDSC differentiation and lung cancer progression by CXCL10 blockade and STING overexpression. (A) BMCs and D122 lung cancer cell culture supernatants were co-cultured with CXCL10 neutralizing antibody, and the differentiation of BMCs into MDSCs was assessed by flow cytometry. (B) The viability of D122 cells co-cultured with BMCs and CXCL10 neutralizing antibody was measured using the CCK-8 assay. (C) D122 cell invasion was evaluated by Transwell assay under the same co-culture conditions with CXCL10 neutralizing antibody, and the invasion rate was quantitatively analyzed. Representative images were captured at 200× magnification with a scale bar of 200 μm. STING, stimulator of interferon gene; CXCL10, IFN-gamma-inducible protein 10; BMC, bone marrow cell; MDSC, myeloid-derived suppressor cell; NC, negative control. Data are presented as mean ± SD (n = 3). *$p < 0.05$, **$p < 0.01$, ***$p < 0.001$.

was reversed by NAb-CXCL10 (Fig. 4A, $p < 0.001$). Co-culture with BMCs enhanced D122 cell viability and invasion (Fig. 4B,C, $p < 0.01$), which were reduced by STING overexpression; NAb-CXCL10 reversed these effects (Fig. 4B,C, $p < 0.05$). These results suggest that STING overexpression inhibits macrophage polarization toward the M2 phenotype and reduces MDSC differentiation through CXCL10-dependent mechanisms.

Discussion

In this study, we identified the role of STING in regulating macrophage polarization and BMC differentiation, highlighting the key cytokine CXCL10 and validating the importance of the TME in lung cancer research. Under normal physiological conditions, STING remains inactive. Upon detection of abnormal DNA, the signaling molecule STING is activated via cyclic GMP–AMP synthase (cGAS), which catalyzes the formation of cyclic GMP-AMP (cGAMP) from GTP and ATP. Activated STING then induces the release of chemokines and other factors to mediate immune responses and exert anti-tumor effects [20,21]. A previous study has reported STING silencing in Kras mutant lung cancers [22]. Consistent with these findings, our results showed that STING was downregulated and its signaling pathway inactivated in lung cancer cell lines. Overexpression of STING in these cells led to changes that inhibited tumor progression, providing new insights into the anti-tumor mechanism of STING through modulation of the microenvironment. Interestingly, despite a decrease in *STING* mRNA levels, total protein levels did not show a corresponding reduction, suggesting potential post-transcriptional regulation, which warrants further investigation in future studies.

In general, the malignant development of cancer cells is often accompanied by defects in the cGAS-STING pathway [23]. A study of tumor and immune cell co-cultures found that downregulation of the cGAS-STING pathway in tumor cells caused reduced immune cell infiltration and decreased downstream IFN-I expression [24].

Our study found that inhibiting STING expression in lung cancer cells significantly promotes tumor-associated macrophage polarization toward the M2 phenotype. This is consistent with previous reports demonstrating that suppression of STING expression in cancer cells facilitates M2 macrophage polarization within the TME [25,26]. Conversely, Li *et al*. [27] reported that activation of the STING pathway in cancer cells mobilizes downstream IFN-I, promoting macrophage M1 polarization and inducing apoptosis in lung adenocarcinoma tumors. IFN-I is a critical regulator of both innate and adaptive immunity and a key component of the cGAS-STING pathway [28]. Among IFN-1 family members, IFN-β has been shown to induce the expression of the chemokine CXCL10 in macrophages [29]. Our results further suggest that CXCL10 acts as a downstream cytokine of the STING pathway, mediating STING's regulation of macrophage polarization within the lung cancer TME. These findings provide new experimental evidence for the regulatory role of the STING signaling pathway in shaping the tumor microenvironment.

Our research revealed that silencing the STING gene in lung cancer cells promotes not only macrophage polarization but also the differentiation of BMCs toward MDSCs. This finding confirms the cross-talk between macrophages and MDSCs, where MDSCs enhance macrophage polarization toward the immunosuppressive M2 phenotype within the TME [30]. More importantly, it highlights the pivotal role of STING signaling in regulating these two immunosuppressive cell populations. At the onset of cancer, MDSCs are recruited to the site of pathology, where they suppress the function of normal immune effector cells [31,32]. Consistent with the report by Mohamed *et al*. [33] showing that conditional knockout of STING restores the immunosuppressive potential of MDSCs, our study further clarifies the direct regulatory role of STING in MDSC differentiation within the lung cancer microenvironment. Additionally, prior studies have shown that activation of STING signaling in cancer cells can support anti-tumor immune responses by inhibiting and reprogramming MDSCs in the TME [33,34]. Our findings also demonstrate that STING activation in lung cancer cells stimulates the upregulation of downstream CXCL10, which may be a key mechanism to alleviate MDSC-mediated immune suppression. This provides a novel molecular explanation supporting existing literature.

The role of chemokine CXCL10 in the TME has been widely studied. Limagne *et al*. [35] found that inhibition of Mitogen-activated protein kinase kinase (MEK) in lung tumors promotes mitochondrial autophagy, induces CXCL10 production and improves the effect of chemotherapy. In fibrotic hepatocellular carcinoma, CXCL10 was able to regulate the TME, especially the infiltration effect of anti-tumor immune cells [36]. In our study, overexpression of STING in lung cancer cell lines upregulated CXCL10, which influenced macrophage polarization and BMC differentiation within the TME. The STING/CXCL10 axis appears to precisely inhibit tumor infiltration and metastasis while promoting tumor apoptosis by modulating and reprogramming immune cells in the TME. Notably, M0 macrophages and BMCs were found to enhance the malignant behavior of lung cancer cells, and these effects were regulated by the STING/CXCL10 axis. These findings suggest that targeting the STING pathway could be a promising strategy to reprogram immune cells in the TME, thereby improving the efficacy of current lung cancer therapies and reducing tumor progression.

While this study add a new direction for thinking about anti-tumor immunotherapy and suggest that the STING/CXCL10 axis is a potential target for lung cancer therapy, several limitations remain. First, the findings

are primarily based on *in vitro* experiments, animal experiments can be added to later studies to verify whether these findings are equally feasible *in vivo*. Moreover, although STING has shown immunomodulatory effects in various tumors, its therapeutic efficacy and safety in lung cancer patients need further investigation using human-derived cell lines or patient tumor samples. Additionally, monoculture experiments could help differentiate tumor cell-autonomous effects from immune-mediated mechanisms, which we plan to explore in future studies.

Conclusions

This study revealed the critical regulatory role of the STING/CXCL10 axis in the lung cancer microenvironment by inhibiting macrophage M2 polarization and blocking the differentiation of BMCs into MDSCs. These findings provide a new direction for developing targeted strategies that modulate tumor-immune cell interactions in lung cancer therapy. Our results suggest that the STING/CXCL10 axis represents a promising therapeutic target for lung cancer treatment.

Availability of Data and Materials

The analyzed data sets generated during the study are available from the corresponding author on reasonable request.

Author Contributions

Substantial contributions to conception and design: HJL. Data acquisition, data analysis and interpretation: DFZ, JJR, JDL, SSH and JY. JY has been involved in drafting the manuscript. All authors have been involved in revising the manuscript critically for important intellectual content. Final approval of the version to be published: All authors. Agreement to be accountable for all aspects of the work in ensuring that questions related to the accuracy or integrity of the work are appropriately investigated and resolved: All authors.

Ethics Approval and Consent to Participate

All mouse treatments were carried out in accordance with the China Council on Animal Care and Use guidelines and were approved by the Ethics Committee of Zhejiang Baiyue Biotech Co., Ltd. for Experimental Animals Welfare (NO. ZJBYLA-IACUC-20230622).

Acknowledgment

Not applicable.

Funding

This work was supported by Medical Scientific Research Foundation of Zhejiang Province, China (No. 2019KY593), Ningbo Natural Science Foundation, China (No. 202003N4277), Ningbo Clinical Research Center for Respiratory Diseases (No. 2022L004), Ningbo Health Branding Subject Fund (No. PPXK2018-05) and Ningbo Municipal Key clinical specialty in Respiratory Medicine (No. 2025002).

Conflict of Interest

The authors declare no conflict of interest.

Supplementary Material

Supplementary material associated with this article can be found, in the online version, at https://doi.org/10.24976/Discov.Med.202537201.202.

References

[1] Ferlay J, Colombet M, Soerjomataram I, Parkin DM, Piñeros M, Znaor A, *et al*. Cancer statistics for the year 2020: An overview. International Journal of Cancer. 2021. https://doi.org/10.1002/ijc.33588.

[2] Bray F, Laversanne M, Sung H, Ferlay J, Siegel RL, Soerjomataram I, *et al*. Global cancer statistics 2022: GLOBOCAN estimates of incidence and mortality worldwide for 36 cancers in 185 countries. CA: a Cancer Journal for Clinicians. 2024; 74: 229–263. https://doi.org/10.3322/caac.21834.

[3] Liu W, Powell CA, Wang Q. Tumor microenvironment in lung cancer-derived brain metastasis. Chinese Medical Journal. 2022; 135: 1781–1791. https://doi.org/10.1097/CM9.0000000000002127.

[4] Huang F, He K. Rhizoma Zedoariae Inhibits G-CSF-Induced MDSCs-like Differentiation of THP-1 Cells. Journal of Experimental and Clinical Application of Chinese Medicine. 2024; 5: 12–22. https://doi.org/10.62767/jecacm503.1126.

[5] de Visser KE, Joyce JA. The evolving tumor microenvironment: From cancer initiation to metastatic outgrowth. Cancer Cell. 2023; 41: 374–403. https://doi.org/10.1016/j.ccell.2023.02.016.

[6] Hu J, Sánchez-Rivera FJ, Wang Z, Johnson GN, Ho YJ, Ganesh K, *et al*. STING inhibits the reactivation of dormant metastasis in lung adenocarcinoma. Nature. 2023; 616: 806–813. https://doi.org/10.1038/s41586-023-05880-5.

[7] Huang R, Ning Q, Zhao J, Zhao X, Zeng L, Yi Y, *et al*. Targeting STING for cancer immunotherapy: From mechanisms to translation. International Immunopharmacology. 2022; 113: 109304. https://doi.org/10.1016/j.intimp.2022.109304.

[8] Jiang M, Chen P, Wang L, Li W, Chen B, Liu Y, *et al*. cGAS-STING, an important pathway in cancer immunotherapy. Journal of Hematology & Oncology. 2020; 13: 81. https://doi.org/10.1186/s13045-020-00916-z.

[9] Wang Q, Bergholz JS, Ding L, Lin Z, Kabraji SK, Hughes ME, *et al*. STING agonism reprograms tumor-associated macrophages and overcomes resistance to PARP inhibition in BRCA1-deficient models of breast cancer. Nature Communications. 2022; 13: 3022. https://doi.org/10.1038/s41467-022-30568-1.

[10] Tani T, Mathsyaraja H, Campisi M, Li ZH, Haratani K, Fahey CG, *et al*. TREX1 Inactivation Unleashes Cancer Cell STING-Interferon Signaling and Promotes Antitumor Immunity. Can-

cer Discovery. 2024; 14: 752–765. https://doi.org/10.1158/2159-8290.CD-23-0700.

[11] Taniguchi H, Caeser R, Chavan SS, Zhan YA, Chow A, Manoj P, *et al*. WEE1 inhibition enhances the antitumor immune response to PD-L1 blockade by the concomitant activation of STING and STAT1 pathways in SCLC. Cell Reports. 2022; 39: 110814. https://doi.org/10.1016/j.celrep.2022.110814.

[12] Liu C, Zheng S, Wang Z, Wang S, Wang X, Yang L, *et al*. KRAS-G12D mutation drives immune suppression and the primary resistance of anti-PD-1/PD-L1 immunotherapy in non-small cell lung cancer. Cancer Communications (London, England). 2022; 42: 828–847. https://doi.org/10.1002/cac2.12327.

[13] Ribas A, Wolchok JD. Cancer immunotherapy using checkpoint blockade. Science (New York, N.Y.). 2018; 359: 1350–1355. https://doi.org/10.1126/science.aar4060.

[14] Jie X, Chen Y, Zhao Y, Yang X, Xu Y, Wang J, *et al*. Targeting KDM4C enhances $CD8^+$ T cell mediated antitumor immunity by activating chemokine CXCL10 transcription in lung cancer. Journal for Immunotherapy of Cancer. 2022; 10: e003716. https://doi.org/10.1136/jitc-2021-003716.

[15] Yu L, Huang K, Liao Y, Wang L, Sethi G, Ma Z. Targeting novel regulated cell death: Ferroptosis, pyroptosis and necroptosis in anti-PD-1/PD-L1 cancer immunotherapy. Cell Proliferation. 2024; 57: e13644. https://doi.org/10.1111/cpr.13644.

[16] Pritchard A, Tousif S, Wang Y, Hough K, Khan S, Strenkowski J, *et al*. Lung Tumor Cell-Derived Exosomes Promote M2 Macrophage Polarization. Cells. 2020; 9: 1303. https://doi.org/10.3390/cells9051303.

[17] Wei H, Guo C, Zhu R, Zhang C, Han N, Liu R, *et al*. Shuangshen granules attenuate lung metastasis by modulating bone marrow differentiation through mTOR signalling inhibition. Journal of Ethnopharmacology. 2021; 281: 113305. https://doi.org/10.1016/j.jep.2020.113305.

[18] Maren NA, Duduit JR, Huang D, Zhao F, Ranney TG, Liu W. Stepwise Optimization of Real-Time RT-PCR Analysis. Methods in Molecular Biology (Clifton, N.J.). 2023; 2653: 317–332. https://doi.org/10.1007/978-1-0716-3131-7_20.

[19] House IG, Savas P, Lai J, Chen AXY, Oliver AJ, Teo ZL, *et al*. Macrophage-Derived CXCL9 and CXCL10 Are Required for Antitumor Immune Responses Following Immune Checkpoint Blockade. Clinical Cancer Research: an Official Journal of the American Association for Cancer Research. 2020; 26: 487–504. https://doi.org/10.1158/1078-0432.CCR-19-1868.

[20] Samson N, Ablasser A. The cGAS-STING pathway and cancer. Nature Cancer. 2022; 3: 1452–1463. https://doi.org/10.1038/s43018-022-00468-w.

[21] Kwon J, Bakhoum SF. The Cytosolic DNA-Sensing cGAS-STING Pathway in Cancer. Cancer Discovery. 2020; 10: 26–39. https://doi.org/10.1158/2159-8290.CD-19-0761.

[22] Kitajima S, Ivanova E, Guo S, Yoshida R, Campisi M, Sundararaman SK, *et al*. Suppression of STING Associated with LKB1 Loss in KRAS-Driven Lung Cancer. Cancer Discovery. 2019; 9: 34–45. https://doi.org/10.1158/2159-8290.CD-18-0689.

[23] Li A, Yi M, Qin S, Song Y, Chu Q, Wu K. Activating cGAS-STING pathway for the optimal effect of cancer immunotherapy. Journal of Hematology & Oncology. 2019; 12: 35. https://doi.org/10.1186/s13045-019-0721-x.

[24] Tan YS, Sansanaphongpricha K, Xie Y, Donnelly CR, Luo X, Heath BR, *et al*. Mitigating SOX2-potentiated Immune Escape of Head and Neck Squamous Cell Carcinoma with a STING-inducing Nanosatellite Vaccine. Clinical Cancer Research: an Official Journal of the American Association for Cancer Research. 2018; 24: 4242–4255. https://doi.org/10.1158/1078-0432.CCR-17-2807.

[25] Su W, Gao W, Zhang R, Wang Q, Li L, Bu Q, *et al*. TAK1 deficiency promotes liver injury and tumorigenesis via ferroptosis and macrophage cGAS-STING signalling. JHEP Reports: Innovation in Hepatology. 2023; 5: 100695. https://doi.org/10.1016/j.jhepr.2023.100695.

[26] Geng K, Ma X, Jiang Z, Huang W, Gu J, Wang P, *et al*. High glucose-induced STING activation inhibits diabetic wound healing through promoting M1 polarization of macrophages. Cell Death Discovery. 2023; 9: 136. https://doi.org/10.1038/s41420-023-01425-x.

[27] Li Y, Gao Y, Jiang X, Cheng Y, Zhang J, Xu L, *et al*. SAMHD1 silencing cooperates with radiotherapy to enhance anti-tumor immunity through IFI16-STING pathway in lung adenocarcinoma. Journal of Translational Medicine. 2022; 20: 628. https://doi.org/10.1186/s12967-022-03844-3.

[28] Si W, Liang H, Bugno J, Xu Q, Ding X, Yang K, *et al*. *Lactobacillus rhamnosus* GG induces cGAS/STING- dependent type I interferon and improves response to immune checkpoint blockade. Gut. 2022; 71: 521–533. https://doi.org/10.1136/gutjnl-2020-323426.

[29] Makuch E, Jasyk I, Kula A, Lipiński T, Siednienko J. IFNβ-Induced *CXCL10* Chemokine Expression Is Regulated by Pellino3 Ligase in Monocytes and Macrophages. International Journal of Molecular Sciences. 2022; 23: 14915. https://doi.org/10.3390/ijms232314915.

[30] Sinha P, Clements VK, Bunt SK, Albelda SM, Ostrand-Rosenberg S. Cross-talk between myeloid-derived suppressor cells and macrophages subverts tumor immunity toward a type 2 response. Journal of Immunology (Baltimore, Md.: 1950). 2007; 179: 977–983. https://doi.org/10.4049/jimmunol.179.2.977.

[31] Yang Z, Guo J, Weng L, Tang W, Jin S, Ma W. Myeloid-derived suppressor cells-new and exciting players in lung cancer. Journal of Hematology & Oncology. 2020; 13: 10. https://doi.org/10.1186/s13045-020-0843-1.

[32] Bruno A, Mortara L, Baci D, Noonan DM, Albini A. Myeloid Derived Suppressor Cells Interactions With Natural Killer Cells and Pro-angiogenic Activities: Roles in Tumor Progression. Frontiers in Immunology. 2019; 10: 771. https://doi.org/10.3389/fimmu.2019.00771.

[33] Mohamed E, Sierra RA, Trillo-Tinoco J, Cao Y, Innamarato P, Payne KK, *et al*. The Unfolded Protein Response Mediator PERK Governs Myeloid Cell-Driven Immunosuppression in Tumors through Inhibition of STING Signaling. Immunity. 2020; 52: 668–682.e7. https://doi.org/10.1016/j.immuni.2020.03.004.

[34] Cheng H, Xu Q, Lu X, Yuan H, Li T, Zhang Y, *et al*. Activation of STING by cGAMP Regulates MDSCs to Suppress Tumor Metastasis *via* Reversing Epithelial-Mesenchymal Transition. Frontiers in Oncology. 2020; 10: 896. https://doi.org/10.3389/fonc.2020.00896.

[35] Limagne E, Nuttin L, Thibaudin M, Jacquin E, Aucagne R, Bon M, *et al*. MEK inhibition overcomes chemoimmunotherapy resistance by inducing CXCL10 in cancer cells. Cancer Cell. 2022; 40: 136–152.e12. https://doi.org/10.1016/j.ccell.2021.12.009.

[36] Brandt EF, Baues M, Wirtz TH, May JN, Fischer P, Beckers A, *et al*. Chemokine CXCL10 Modulates the Tumor Microenvironment of Fibrosis-Associated Hepatocellular Carcinoma. International Journal of Molecular Sciences. 2022; 23: 8112. https://doi.org/10.3390/ijms23158112.